ACS APPLIED MATERIALS & INTERFACES

www.acsami.org

Research Article

Investigation of Electrolyte-Dependent Carbonate Formation on Gas Diffusion Electrodes for CO_2 Electrolysis

Emiliana R. Cofell, Uzoma O. Nwabara, Saket S. Bhargava, Danielle E. Henckel, and Paul J. A. Kenis*

Cite This: *ACS Appl. Mater. Interfaces* 2021, 13, 15132–15142

Read Online

ACCESS | Metrics & More | Article Recommendations | Supporting Information

ABSTRACT: The electrochemical reduction of CO_2 (ECO_2R) is a promising method for reducing CO_2 emissions and producing carbon-neutral fuels if long-term durability of electrodes can be achieved by identifying and addressing electrode degradation mechanisms. This work investigates the degradation of gas diffusion electrodes (GDEs) in a flowing, alkaline CO_2 electrolyzer via the formation of carbonate deposits on the GDE surface. These carbonate deposits were found to impede electrode performance after only 6 h of operation at current densities ranging from −50 to −200 mA cm^{-2}. The rate of carbonate deposit formation on the GDE surface was determined to increase with increasing electrolyte molarity and became more prevalent in K^+-containing as opposed to Cs^+-containing electrolytes. Electrolyte composition and concentration also had significant effects on the morphology, distribution, and surface coverage of the carbonate deposits. For example, carbonates formed in K^+-containing electrolytes formed concentrated deposit regions of varying morphology on the GDE surface, while those formed in Cs^+-containing electrolytes appeared as small crystals, well dispersed across the electrode surface. Both deposits occluding the catalyst layer surface and those found within the microporous layer and carbon fiber substrate of the electrode were found to diminish performance in ECO_2R, leading to rapid loss of CO production after ∼50% of the catalyst layer surface was occluded. Additionally, carbonate deposits reduced GDE hydrophobicity, leading to increased flooding and internal deposits within the GDE substrate. Electrolyte engineering-based solutions are suggested for improved GDE durability in future work.

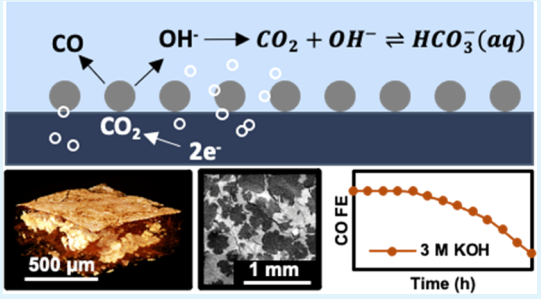

KEYWORDS: *CO_2 electroreduction, durability, flow cell, carbonate formation, degradation mechanisms*

1. INTRODUCTION

1.1. Background. The electrochemical reduction of carbon dioxide (CO_2) (ECO_2R) is a promising technology for the production of intermediates for high-energy-density fuels and commodity chemicals in a carbon-neutral manner using renewable energy; currently, these chemicals are produced via carbon-intensive methods, often using nonrenewable feedstocks.[1] The implementation of ECO_2R combined with other technologies to reduce anthropogenic CO_2 emissions is essential to combat climate change, which currently threatens widespread damage to the earth's ecosystems and human communities.[2,3]

Prior work by many research groups has led to the discovery of several primary catalysts that exhibit high activity and stability for products such as carbon monoxide (CO), formate, ethylene (C_2H_4), and ethanol (C_2H_5OH).[1,4] Many of these catalysts are now being evaluated for performance and durability in scalable cell configurations including flow electrolyzer and membrane electrode assembly (MEA)-based systems. Traditional and flow-based electrochemical systems using silver- or gold-based nanoparticle catalysts are routinely able to achieve ≥90% faradic efficiency (FE) for CO production.[5,6] Notable results have been achieved for conversion to C_2 products on copper-based catalysts; for example, Hoang et al. reported 60% FE for C_2H_4 and 25% for C_2H_5OH on a copper−silver alloy.[7] Recent efforts to create MEA-based ECO_2R electrolyzers may further aid in maintaining high performance over thousands of hours.[8,9]

Both MEA-based and flow cell electrolysis systems rely on gas diffusion electrodes (GDEs) to overcome low solubility and mass transport limitations of CO_2 in aqueous electrolytes. GDEs are composed of (i) a catalyst layer (CL) containing the catalyst and a polymer binder such as Nafion, which provides stability and hydrophobicity, (ii) a microporous layer (MPL), where a hydrophobic polymer such as poly(tetrafluoroethylene) (PTFE) is mixed with carbon to resist the incursion of liquid past the catalyst layer, and (iii) a carbon fiber substrate (CFS) for mechanical stability, also wet-proofed with PTFE.[10] Figure 1a shows the flow of liquid and gas in the

Received: December 11, 2020
Accepted: March 2, 2021
Published: March 25, 2021

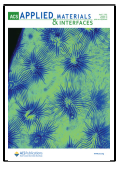

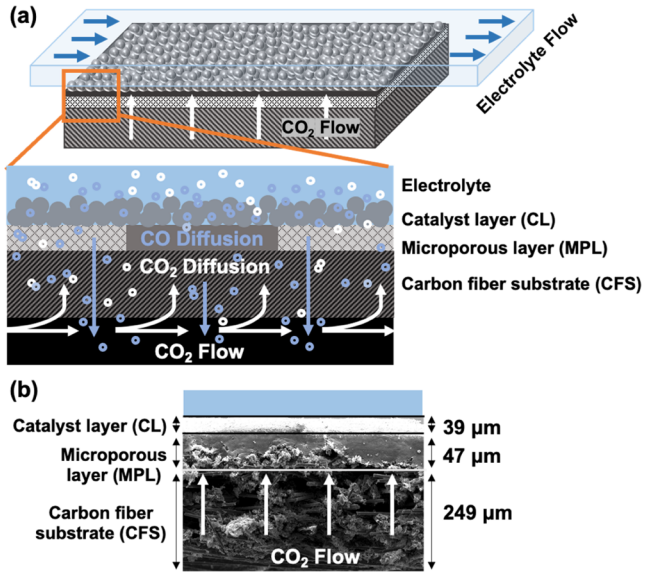

Figure 1. (a) Schematic of the layers of a typical GDE including the carbon fiber substrate, a microporous layer composed of carbon and PTFE, and the catalyst layer. Gaseous CO_2 diffuses through the back of the electrode, while the catalyst layer is in contact with the liquid electrolyte. (b) Modified SEM cross section of a Ag-coated Sigracet 35 BC GDE substrate with a thickness of each layer indicated.

layer of the GDE, while Figure 1b shows an enhanced scanning electron microscopy (SEM) cross section of the CL, MPL, and CFS. During operation, gaseous CO_2 diffuses through the CFS and MPL to the CL, where it comes in contact with the catalyst and a flowing, liquid electrolyte, allowing the ECO_2R reaction to occur at the triple phase boundary (TPB). While this description is somewhat of an oversimplification, the TPB model highlights the need to maintain MPL and CL hydrophobicity for the continued reduction of CO_2 to ECO_2R products.[11]

To date, only a few GDE-based systems have been operated successfully for extended periods of time. Benchmarks for the ECO_2R system durability, to achieve technoeconomic feasibility, range from 3000 to 20 000 h.[12−14] In our review of durability in these systems, we found that the majority of ECO_2R systems reported to date are tested for 10 h or fewer.[15] Exceptions include dioxide materials' MEA-based setup, which converts CO_2 to CO for 6 months (4380 h) at a current density of −50 mA cm^{-2}, and Siemens' flow electrolyzer, which converts CO_2 to syngas for 1200 h at a current density of −300 mA cm^{-2}. These long-term studies, however, also exhibited gradual drops in performance. For most of these durability studies, short or long, detailed insight into the physical and chemical mechanisms causing gradual degradation of the GDEs is still lacking.

1.2. CO_2 and Alkaline Media. Flow electrolyzer systems employing GDEs are commonly operated in alkaline conditions due to suppression of the competing hydrogen evolution reaction (HER) at pH > 12 and the fact that highly conductive alkaline electrolytes such as potassium hydroxide (KOH) improve ECO_2R kinetics, leading to higher current densities for a given cell potential than neutral electrolytes.[16,17] In an alkaline environment, CO_2 will react to form carbonate and bicarbonate compounds in an alkaline solution via reactions 1 and 2: first, CO_2 reacts with OH^- to form bicarbonate (HCO_3^-); second, bicarbonate is deprotonated by a hydroxide to form a carbonate (CO_3^{2-}) and water

$$CO_2 + OH^- \rightleftharpoons HCO_3^-(aq) \quad (1)$$

$$HCO_3^-(aq) + OH^- \rightleftharpoons CO_3^{2-}(aq) + H_2O \quad (2)$$

Carbonate formation presents an issue in a variety of applications, for example, the formation of calcium carbonate scale in water purification systems.[18] The natural uptake of CO_2 by the oceans, which acts as a buffer to some anthropogenic CO_2 emissions, leads to gradual ocean acidification by the formation of HCO_3^-.[19] In electrochemical systems such as alkaline fuel cells or CO_2 electrolyzers, carbonate deposits can form directly on the electrode, blocking the catalyst surface, thereby hampering transport and reducing the number of available active sites.[20−24] A recent paper by Leonard et al. explored carbonate formation on GDEs as the dominant factor leading to flooding in a flow electrolyzer; flooding is a process by which liquid penetrates the hydrophobic MPL, moving the TPB away from the catalyst layer and eventually halting the reaction.[25] Additionally, Rabinowitz and Kanan recently commented on the detrimental impact of carbonate formation on energy efficiency in low-temperature ECO_2R systems.[26] However, to date, the specific conditions leading to promotion or inhibition of carbonate formation on GDEs and growth rate of carbonate deposits in alkaline flow ECO_2R systems have not been studied.

Our work reported here provides an in-depth look at the way by which carbonate deposit formation influences GDE performance under various electrolyte conditions when converting CO_2 to CO at high current densities (−50 to −200 mA cm^{-2}). We use a thorough pre-and-post-testing characterization protocol employing SEM, energy-dispersive X-ray spectroscopy (EDX), X-ray diffraction spectrometry (XRD), and other techniques to investigate the role of electrolyte concentration and composition on the formation of carbonate deposits on the Ag-coated GDEs. We show that the widespread deposition of carbonate on the catalyst layer is responsible for electrode performance degradation and that carbonate-forming reactions are driven by both increasing electrolyte molarity and increasing applied current density. Additionally, we observe a change in carbonate deposit morphology when switching electrolyte cation from K^+ to Cs^+. We believe that switching to a larger cation (Cs^+) results in more well-dispersed carbonate crystals, this slowing but not eliminating carbonate-related performance degradation at high electrolyte concentrations. Finally, we show that these carbonate deposits may facilitate penetration of the electrolyte into layers of the GDE via loss of catalyst layer hydrophobicity, resulting in further GDE degradation.

2. ELECTROCHEMICAL TESTING AND CHARACTERIZATION METHODS

2.1. Electrode Preparation. The cathodes were prepared in batches of 4 by sonicating 10 mg of Ag nanopowder (Sigma-Aldrich, <150 nm particle size, 99% trace metal basis) with 300 μL of deionized water, 26 μL of Nafion (5 wt % Fuel Cell Earth) binder, and 300 μL of isopropyl alcohol (IPA) for 20−30 min. This ink was airbrushed onto a Sigracet 35 BC GDE (Fuel Cell Store) carbon paper substrate to obtain a loading of 0.5 mg cm^{-2} (±10%), with the custom airbrushing setup described previously.[27] Next, the cathodes were cut into approximately 1 cm × 2.5 cm rectangles to fit into the flow cell. The area used in each reaction was held constant at 1 cm^2—

https://doi.org/10.1021/acsami.0c21997
ACS Appl. Mater. Interfaces 2021, 13, 15132−15142

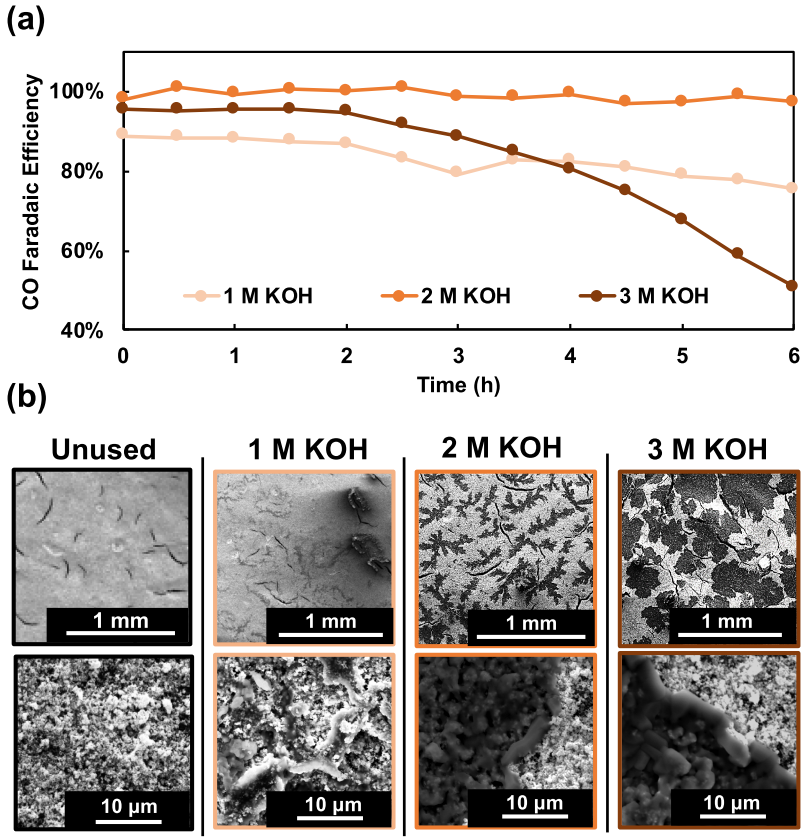

Figure 2. (a) Plot of CO FE over time for each of the GDEs during the electrochemical testing (freshly prepared 0.5 mg cm^{-2} Ag-coated GDEs were tested in each electrolyte for 6 h at a −200 mA cm^{-2} constant current); (b) SEM images (80× magnification top row and 500× bottom row) of the surface of each of four GDEs, one pristine and three that were tested for 6 h in 1, 2, and 3 M KOH, respectively.

both the gas flow chamber and electrolyte flow chamber measure 0.5 cm × 2 cm.

Anodes were prepared in a similar manner, using iridium(IV) oxide nanoparticles (Alfa Aesar, nonhydrate). The anode ink was prepared by mixing 80 mg of IrO_2 nanoparticles with 256 μL of Nafion binder and about 2400 mL each of deionized water and IPA. The ink was airbrushed to obtain an anode loading of 4 mg cm^{-2} (±10%).

2.2. Electrochemical Cell. All of our experiments were carried out in custom electrochemical flow cells designed by our lab and manufactured by the machine shop at UIUC. The flow cell design, pictured in Figure S1, includes a stainless steel cathode and gas flow chamber, a polyether ether ketone (PEEK) electrolyte flow chamber, and a stainless steel anode chamber. All tubing is 0.5 mm in diameter. For each experiment, the cell was assembled using a silicone gasket around the cathode to maintain an airtight environment for the cathode reaction and manually clamped together. Polyethylene tubing was used for both gas and electrolyte flow. More information on cell assembly and design can be found in the Supporting Information.

2.3. Electrolysis Operation Conditions. An electrolyte flow rate of 1 mL min^{-1} was established using a peristaltic pump (Cole Parmer Masterflex L/S). CO_2 was flowed into the cell using a mass flow controller (Cole Parmer) at a rate of 17 sccm. A Ag/AgCl reference electrode (Basi RE-5B) fitted with a porous frit was connected to the electrolyte inlet tube. The active area of each electrode was 1 cm^2 during testing. Current was applied, and cell potential was measured using a potentiostat (Metrohm Autolab PGSTAT302N). Gas products were collected and analyzed using a gas chromatograph (Thermo Finnegan Trace GC) furnished with a thermal conductivity detector.

CO_2 electroreduction was carried out using a variety of electrolytes (all salts purchased from Sigma-Aldrich); 1, 2, and 3 M KOH were prepared using semiconductor-grade ultrapure (99.9%) KOH pellets, 1, 2, and 3 M cesium hydroxide (CsOH) were prepared using (99.9%) CsOH powder, 3 M sodium hydroxide (NaOH) was prepared using (≥98%) NaOH powder, 2 M potassium carbonate (K_2CO_3) was prepared using (≥99%) K_2CO_3 powder, and 2 M potassium bicarbonate ($KHCO_3$) was prepared using (99.7%) $KHCO_3$ powder. For all experiments except where noted, a constant current of −200 mA cm^{-2} was applied to the cell for 6 h. Chronopotentiometry, or operation with a constant applied current, was chosen because the electrochemical responses of the system are easily controlled in this mode. We recorded cathode potential using digital multimeters (Crenova, MS8233D) and assessed the CO FE by using the Thermo Finnegan Trace GC to measure CO and CO_2 at half-hour intervals; the FE was calculated according to the instrument calibration and ratio of CO and CO_2 peaks. More information about the FE calculation can be found in the Supporting Information. After completing each experiment, all cathodes were immediately and thoroughly rinsed with DI water for 10 s each and dried with nitrogen before being stored for characterization.

2.4. Electrode Characterization Protocol. Before testing, fresh electrodes were imaged using SEM (FEI Quanta FEG 450 ESEM); the microscope was operated at 15 kV, and images were taken at 80×, 250×, 500×, 1000×, and 5000× magnifications to compare the overall surface morphology as well as microscale structure after operation in various conditions. Approximately 70% of the used electrode surface was imaged at low magnification. EDX (FEI Quanta FEG 450 ESEM) was performed using the same instrument; each sample was scanned across a surface area of 0.5 and 0.04 mm^2 to compare the presence of carbon, fluorine, silver, and electrolyte cations (K^+, Cs^+, Na+) at various length scales. Sample composition was additionally analyzed using XRD (PANalytical Philips X'pert MRD System #2); the source was operated at 45 kV and 40 mA current. Thirty min scans of each sample were taken; the 2-θ angle was swept from 5 to 100°. XRD peaks were analyzed using Jade software, and peaks were matched with the powder diffraction database from the International Center

https://doi.org/10.1021/acsami.0c21997
ACS Appl. Mater. Interfaces 2021, 13, 15132−15142

for Diffraction Data. In some cases, powder XRD measurements were taken of pure compounds to provide accurate peak matching since some of the alkaline salt compounds we studied were not robustly represented in the database.

Post testing, all of the above measurements (SEM, EDX, XRD) were repeated on the used electrodes. Microcomputed tomography (Micro-CT, Xradia MicroXCT-200) was performed on some of the electrodes to image internal solid deposits; 721 images were taken at 30 kV and 6 W, starting at −180° and rotating to +180°. The three-dimensional (3D) images were reconstructed using XM Reconstructor and XM Viewer software. Finally, contact angle measurements were taken of fresh and used electrodes (Ramé-Hart Model 250 Contact Angle Goniometer) to quantify loss of hydrophobicity in used GDEs.

3. RESULTS AND DISCUSSION

3.1. Durability Testing in KOH Electrolytes. CO_2 reduction was performed in 1, 2, and 3 M KOH. Figure 2a shows the CO FE, which was recorded at half-hour intervals, and Figure 2b shows SEM images of the surface of both an unused electrode and each electrode post testing at 80× and 500× magnifications. The FE for CO remains consistent or declines slowly across all three electrolytes until 2 h when CO production for the 3 M KOH sample begins to rapidly decline (Figure 2a). During the 1 and 2 M tests, we see minor FE fluctuations since operating at high current density results in bubble formation from CO production on the catalyst layer, which can influence product and CO_2 flow rates at the time of GC injection. Additionally, the 2 M test shows overall higher FE than the 1 M test due to higher electrolyte conductivity and pH. The 3 M test begins with similarly high performance, but FE decreases sharply beginning around 2 h of operation. At the end of the 6 h test, the GDEs tested in 1, 2, and 3 M KOH retained a CO FE of 75, 97, and 51%, respectively. The cathode potentials increased over the testing period for the GDEs tested in 2 and 3 M KOH, while the cathode potential did not show an observable trend for the GDE tested in 1 M KOH (Figure S4).

Used electrodes exhibit varying levels of carbonate coverage post testing (Figure 2b). While the surface of the GDE tested in 1 M KOH is free of large-scale blemishes and deposits post testing, it does show smaller deposits that are visible at both high and low magnifications. The surface of the 2 M GDE has more substantial, fractal-like deposits; greater magnification reveals these deposits to be dense, solid regions on top of the Ag catalyst layer. The surface of the 3 M GDE is almost completely covered by deposits that appear similar to those on the surface of the 2 M KOH GDE at high magnification. When correlating the electrochemical performance of each GDE with the post-testing surface images, we can infer that the observed decreases in electrochemical performance are caused by occlusion of the catalyst layer surface by carbonate deposits during the 6 h testing period and that these deposits form more quickly in higher molarity electrolyte.

The relationship between electrolyte molarity and surface deposit coverage can be seen more clearly in Figure 3. MATLAB image analysis of electrodes tested in 1, 2, and 3 M KOH was used to calculate surface coverage by carbonate and shows an increase from around 15% surface coverage of deposits after 6 h of testing in 1 M KOH to around 70% surface coverage after testing in 3 M KOH. Experiments done with 0.5, 1.5, and 2.5 M KOH confirm this trend, in terms of both performance (Figure S2) and surface coverage by deposits (Figure S3). Therefore, testing in 1 M KOH for 6 h

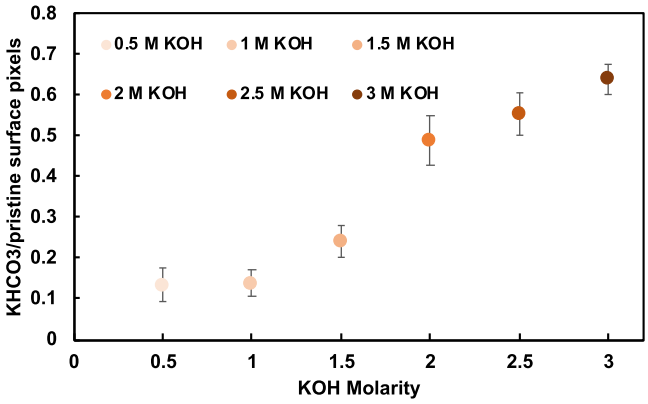

Figure 3. Image analysis performed in MATLAB counting number of pixels assigned to potassium bicarbonate deposits on surface vs total catalyst layer pixels, giving a ratio of surface coverage, for samples run at different KOH molarities. More information on image analysis can be found in the Supporting Information.

results in around 15% surface coverage of carbonate deposits and a 13% loss of FE; testing in 2 M KOH results in around 50% surface coverage and a 3% loss in FE; testing in 3 M KOH results in around 70% surface coverage and 45% loss in FE. This suggests that surface coverage by carbonates is not the only mechanism responsible for degradation in the case of <2 M electrolytes—instead, greater degradation may be related to the higher cathode and cell potentials needed to sustain the applied −200 mA cm^{-2} current density (see the Supporting Information and Table S1). Investigation of degradation modes in low-molarity electrolytes will be the subject of future work; here, we focus on the issue of carbonation formation. We can see that this carbonate-related degradation begins rapidly after more than 50% of the surface is covered by deposits (Figure S3).

The deposits were identified as potassium-rich regions via EDX surface mapping (Figure 4a–d), confirming that they originated from a reaction with the electrolyte. While the unused sample shows only silver from the catalyst layer and carbon from the substrate, the used samples reveal large regions of potassium. More specifically, the deposits were identified as primarily containing potassium bicarbonate ($KHCO_3$) via XRD (Figure 5). This was initially surprising because the rate constant for deprotonation of $KHCO_3$ to potassium carbonate (K_2CO_3) is high ($k = 6.0 \times 10^9$ L mol^{-1} s^{-1}).[11] However, when we investigate the relative solubilities in water at 20 °C, we see that $KHCO_3$ (22.4 g/100 mL) is 5–6 times less soluble than K_2CO_3 (112 g/100 mL),[28] which may explain its greater extent of precipitation.

The effect of applied current on deposit formation was explored by applying a −50 mA cm^{-2} constant current density for 6 h in 3 M KOH and comparing post-testing electrodes to those imaged above (Figure 6a). Additionally, we conducted a control experiment where 17 sccm of CO_2 and 1 mL min^{-1} of 3 M KOH were flowed through the electrochemical cell, but no current was applied. The electrode from the control experiment does not exhibit visible surface deposits, while those on the electrode tested at −50 mA cm^{-2} are less widespread than those on the original sample tested at −200 mA cm^{-2} (Figure 6b). From these results, we hypothesize that both OH^- from the electrolyte and additional OH^- anions produced at the reaction interface by the ECO_2R reaction drive the production of bicarbonate. The bicarbonate locally exceeds

https://doi.org/10.1021/acsami.0c21997
ACS Appl. Mater. Interfaces 2021, 13, 15132−15142

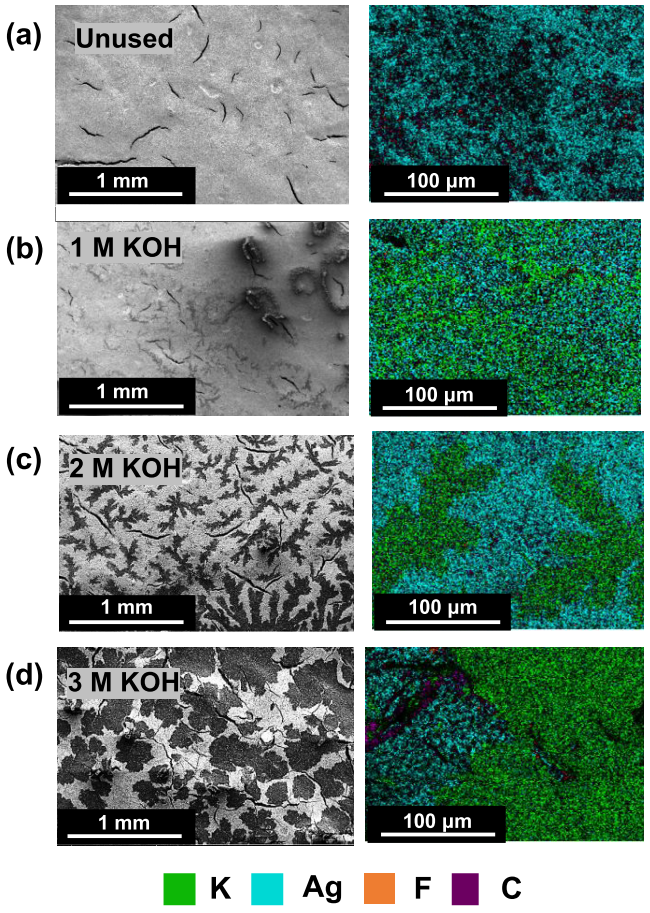

Figure 4. SEM images for scale (left) and EDX images taken at 500× magnification (right), showing the presence of K^+ (corresponding to carbonate and bicarbonate deposits from the electrolyte), Ag (corresponding to the catalyst), F^- (corresponding to the binder used in the catalyst ink), and C (corresponding to the carbon-based Sigracet 35 BC substrate). (a) Pristine electrode pretesting. (b) Electrode tested in 1 M KOH for 6 h. (c) Electrode tested in 2 M KOH for 6 h. (d) Electrode tested in 3 M KOH for 6 h. Each higher-magnification EDX scan was taken from the corresponding lower-magnification SEM image shown, but the scan location is approximate.

its solubility, initiating deposit nucleation and growth on the catalyst layer surface (Figure 6c). Thus, at both higher applied current densities and higher electrolyte concentrations, we see a correspondingly greater amount of carbonate deposits on the electrode surface, accompanied by declining electrochemical performance as the catalyst layer is occluded by these deposits. While we have shown in previous work that increasing from 0.5 to 3 M KOH results in almost a fourfold improvement in CO production,[29] this clearly does not correspond to an increase in durability. By 3 h of testing in 3 M KOH, GDE surface coverage by deposits exceeds 50%, followed by a decline in CO FE that continues for the duration of the test. While deposit morphologies vary (Figure S5), all tested samples experienced catalyst layer occlusion by carbonate deposits.

3.2. Durability Testing in CsOH Electrolytes. Figure 7 shows the performance of GDEs tested in 1, 2, and 3 cesium hydroxide (CsOH). CsOH-based electrolytes have a higher conductivity than KOH-based electrolytes. Additionally, larger cations such as Cs^+ experience less hydration than smaller cations, giving them a higher propensity for adsorption on the electrode surface, which is thought to provide the benefit of stabilizing the CO_2^- intermediate.[30] This leads to improved electroreduction kinetics and lower cell and cathode potentials (higher cell and cathode energy efficiency).[16] Additionally, cesium bicarbonate ($CsHCO_3$) is more soluble than $KHCO_3$ (67.77 g/100 mL H_2O vs 22.4 g/100 mL H_2O),[31,32] which suggests a reduced propensity for deposit formation in Cs-based electrolytes. Therefore, testing the long-term performance of Sigracet GDEs in CsOH was expected to provide important insights regarding the prospects of this electrolyte.

When Ag-coated GDEs were tested in CsOH instead of KOH, we saw several differences in both performance and post-testing characterization. The GDEs tested in 1, 2, and 3 M CsOH retained a CO FE of 88, 108, and 87%, respectively (Figure 7a), corresponding to performance losses of 8.37, 4.86, and 21.8%. The cathode potentials did not exhibit observable trends over the 6 h testing period (Figure S6). The decline in performance in these cathodes also appears to be due to the formation of carbonate deposits on the surface of the catalyst layer, but the deposit morphology differs greatly from those found on the surface of the samples tested in KOH. Visually, the CsOH deposits take the form of small and generally well-dispersed crystals on the surface of the electrode (Figure 7b).

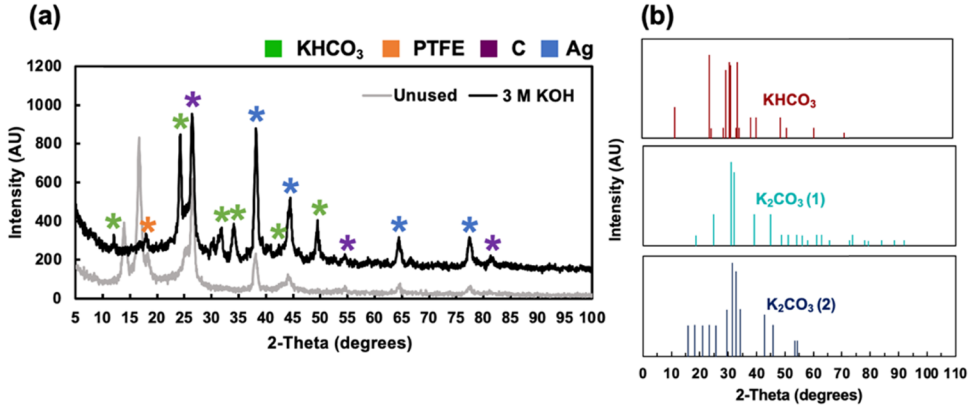

Figure 5. (a) XRD data of an unused sample and a sample tested in 3 M KOH, both for a Ag-coated GDE on a Sigracet 35 BC substrate, with peaks identified as $KHCO_3$, PTFE, C (graphite allotrope), and Ag; (b) patterns from the International Center for Diffraction Database for $KHCO_3$ and two separate records for K_2CO_3, showing that $KHCO_3$ was the best fit for peaks in used samples.

https://doi.org/10.1021/acsami.0c21997
ACS Appl. Mater. Interfaces 2021, 13, 15132−15142

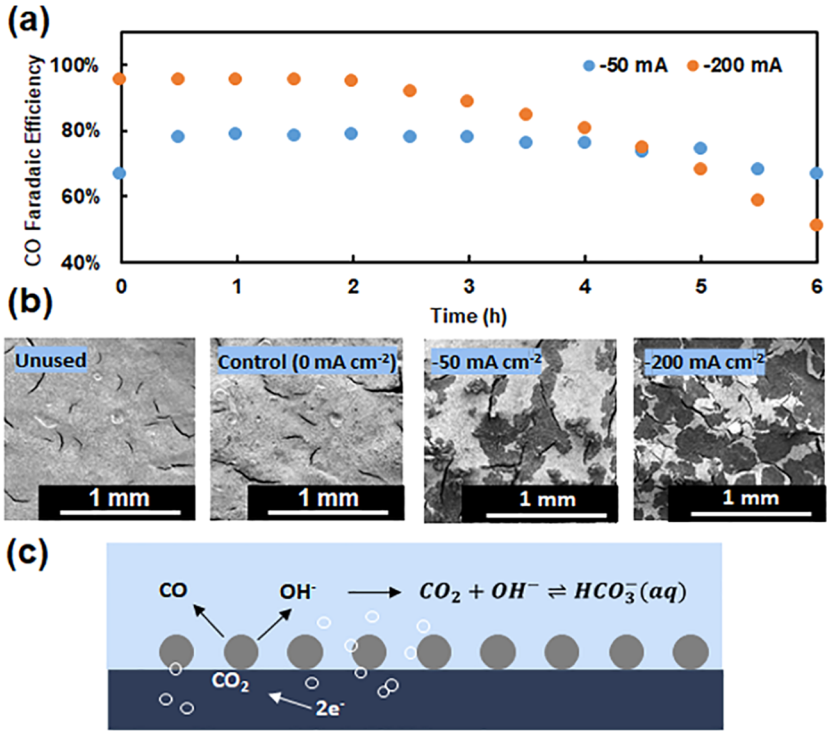

Figure 6. (a) FE data from 6 h of testing in 3 M KOH on two different samples for constant applied currents of −50 and −200 mA cm^{-2}; (b) SEM images taken at 80× magnification of an unused electrode, an electrode used in the control experiment with no applied current, and the −50 and −200 mA cm^{-2} applied current samples. (c) Schematic of the local OH^- production from CO_2 reduction feeding into bicarbonate and carbonate formation.

Crystals of increasing average sizes are observed when increasing the electrolyte concentration from 1 to 2 or 3 M CsOH, but they generally do not form the concentrated regions or fractal-like features seen on the electrodes tested in KOH. Because of the relatively well-dispersed and uniform nature of the small carbonate crystal deposits formed in CsOH, the EDX maps of these samples post testing show a repeatable trend of increasing surface coverage with increasing electrolyte molarity (Figure S8). The samples tested in KOH do not show a similar trend because $KHCO_3$ deposits on the surface are concentrated in dense and irregular regions. On the other hand, the samples tested in CsOH were not suitable for the MATLAB image analysis by the method previously outlined because there was not a high level of contrast between the deposits and the catalyst layer. Overall, the $CsHCO_3$ deposit morphology and even distribution may account for the fact that the performance decrease of the GDE tested in 3 M CsOH is less severe than that of the GDE tested in 3 M KOH since the catalyst layer is less occluded by large-scale deposits.

Multiple factors undoubtedly impact the difference that we observed in deposit morphology and distribution when switching electrolyte cation from K^+ to Cs^+. We believe that the greater solubility of $CsHCO_3$ compared to that of $KHCO_3$ plays a role, as well as the impact of cation size on carbonate deposit nucleation and growth. A comprehensive study comparing the nucleation and growth kinetics of these two compounds does not exist to the best of our knowledge, but kinetic studies done in similar conditions propose several possible explanations. Previous work done on barium sulfate and calcium nucleation and growth in multiple electrolytes suggests that the hydration and radius of the cation play a major role. For smaller and more strongly hydrated cations, the barrier to primary nucleation is higher due to the difficulty of removing water molecules from the ion solvation shell, a first step to crystal formation. This may result in faster nucleation when using a larger and less hydrated cation (Cs^+) and slower nucleation and a higher local concentration of carbonate species when using a smaller cation (K^+). This could explain why we see many small crystals nucleating on the surface of GDEs tested in CsOH, while those tested in KOH grow large deposits from a smaller number of nucleation sites once local solubility limits are exceeded. The lesser degree of coverage of the catalyst layer when using CsOH as an electrolyte may be attributable to the fact that both smaller crystals are more soluble (Ostwald's rule) and $CsHCO_3$ has a higher overall solubility in solution; these kinetics are specific for different electrolyte solutions and should be studied further.

In summary, switching the electrolyte cation from K^+ to Cs^+ enhances the performance and durability when using 3 M electrolytes but does not eliminate the growth of deposits on the catalyst layer and subsequent performance decline due to loss of active area. The interplay of ionic radius, ion hydration, and solubility in K^+- vs Cs^+-containing electrolytes and its impact on the nucleation and growth mechanisms of $KHCO_3$ and $CsHCO_3$ deposits should be studied in detail for a deeper understanding of the effect of electrolyte composition on the durability of GDEs and ECO_2R systems.

3.3. Other Electrolytes. Six hour durability tests at −200 mA cm^{-2} were also performed in 2 M NaOH, 2 M $KHCO_3$, and 2 M K_2CO_3 to further explore the impact of different anions and cations (Figure 8). Na^+ is not a practical cation for extensive testing due to poor solubility, inducing the rapid loss of (initially low) CO FE and frequent blocking of tubes in our cell during testing. Of the anions tested, OH^- showed the best performance; this is likely attributable to the higher pH of 2 M KOH (13.78), compared to those of 2 M K_2CO_3 (12.89) and

https://doi.org/10.1021/acsami.0c21997
ACS Appl. Mater. Interfaces 2021, 13, 15132−15142

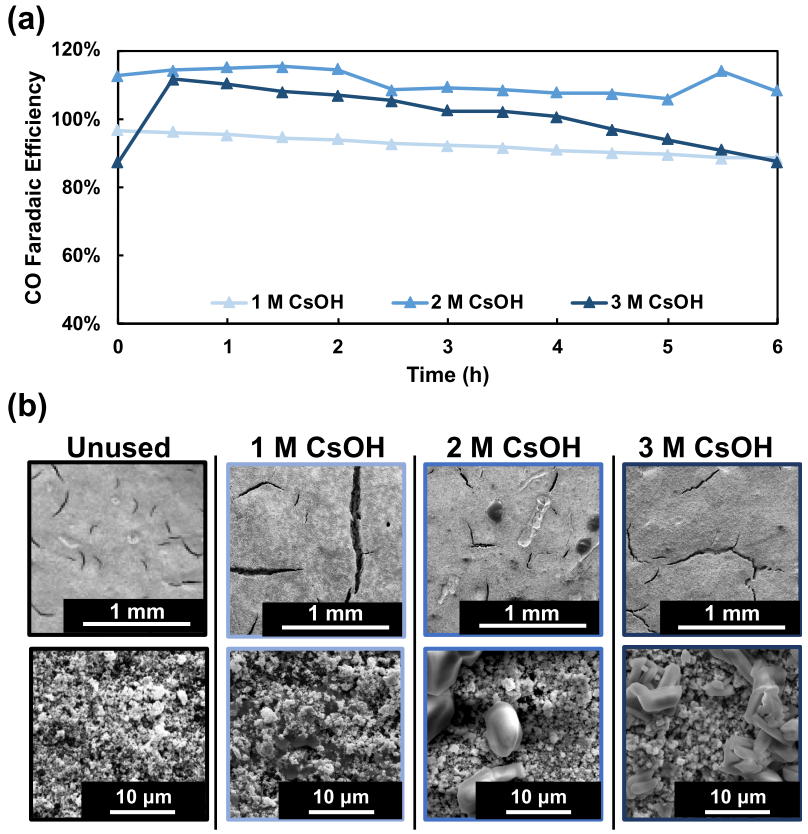

Figure 7. (a) Plot of CO FE over time for each of the GDEs during the electrochemical testing (−200 mA cm^{-2} constant current)—first data point in a 3 M CsOH curve is an outlier due to cell blockage during the beginning of the experiment; (b) SEM images (top 80× magnification and bottom 500× magnification) of the surface of each of four GDEs, one pristine and three that were tested for 6 h in 1, 2, and 3 M CsOH, respectively.

2 M $KHCO_3$ (8.84). Similarly, 2 M KOH has a conductivity of 352 mS cm^{-1}, while 2 M K_2CO_3 and 2 M $KHCO_3$ exhibit lower conductivities at 190 and 100 mS cm^{-1}, respectively.[16,33−35] This correlation is generally reflected in the FE values of these electrolytes, with the more alkaline and more conductive 2 M KOH performing better due to enhanced charge transfer. Samples tested in 2 M K_2CO_3 and 2 M KH_2CO_3 electrolytes showed widespread carbonate deposits on the surface of the catalyst layer (Figure S9). This, together with the data in Figure 8, demonstrates that, of the different alkaline electrolytes tested, GDEs operated in CsOH electrolytes are most promising for long-term operation.

3.4. Characterizing Carbonate Deposits within the GDE. To expand our study of the detrimental impacts of carbonate formation on our GDEs, we took contact angle data both for unused GDEs and for those tested in various electrolytes (Figure 9a). Although our GDE/Ag catalyst layer is initially extremely hydrophobic, exhibiting a contact angle of ∼155° with water, this hydrophobicity is lost after testing for 6 h; the extent of the decrease in contact angle correlates with increasing electrolyte molarity. This can be attributed to the influence of carbonate deposits on the catalyst layer; both $KHCO_3$ and K_2CO_3 contain hydrophilic polar carboxyl groups. The control sample tested in 3 M KOH with no applied current maintained a high contact angle (∼143°) due to the absence of widespread carbonate deposits on the surface, confirming the role of both electrolyte and applied current in deposit formation and degradation.

Additionally, we imaged the internal structure of some of our used electrodes using Micro-CT. Figure 9b compares a pristine GDE to those tested for 6 h in 3 M KOH and 3 M CsOH at −200 mA cm^{-2}. Regions of increased brightness correspond to increased X-ray absorption by dense elements. Initially, the catalyst layer is brightest due to the presence of Ag nanoparticles; in used samples, increased brightness of the catalyst layer and concentrated internal deposits embedded in the MPL/CFS most likely indicate the presence of K^+ and Cs^+. These changes can be due to (1) deposition of potassium bicarbonate on the catalyst layer surface, as previously discussed, and/or (2) formation of potassium-based deposits, most likely potassium bicarbonate, within the layers of the electrode substrate itself, due to flooding.

The phenomenon of flooding in GDEs has been widely studied.[25,36−38] The incursion of liquid can cause the TPB to move away from the catalyst layer and into the substrate. As previously discussed, carbonate anions are highly hydrophilic compared to the Nafion polymer binder in the catalyst layer. The coverage of large portions of the surface by carbonate deposits would greatly decrease hydrophobicity, thus increasing the possibility of flooding events, as aqueous electrolyte is no longer repelled strongly. In all tests in electrolytes with concentrations of 2 M or greater, we observed periodic minor flooding of the electrolyte into the gas outlet, confirming that this is a common issue. In multiple used electrodes imaged via Micro-CT, bright deposits within the electrode structure are evident, likely carbonate deposits. These internal deposits were more prevalent in electrodes tested in KOH compared to those

https://doi.org/10.1021/acsami.0c21997
ACS Appl. Mater. Interfaces 2021, 13, 15132−15142

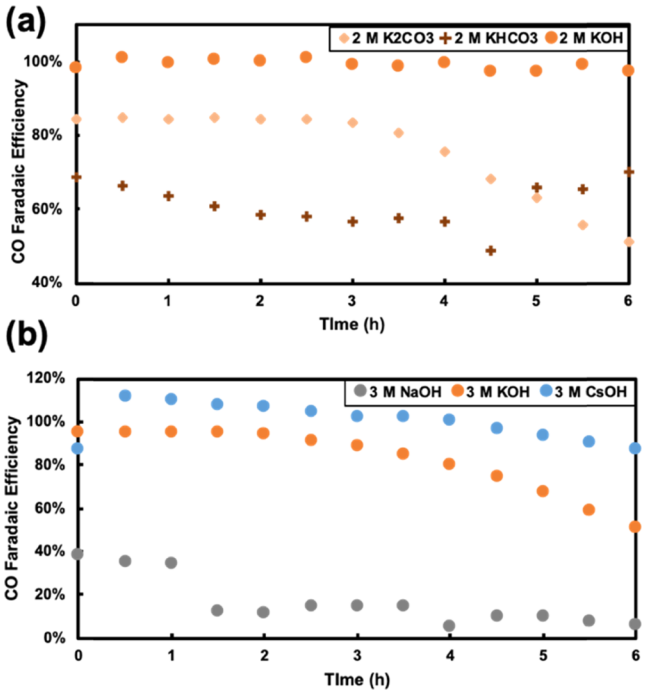

Figure 8. Experiments were done varying the electrolyte anion (a) and cation (b) to compare performance. In (a), we see that samples tested in 2 M K_2CO_3 and 2 M $KHCO_3$ show low FE for CO due to the less alkaline and conductive nature of these electrolytes. The post-testing images of the electrode surfaces show large-scale deposits similar to those found on the surface of the 2 and 3 M KOH electrodes (Figure S9). In (b), the performance in KOH and CsOH is as previously reported, while testing in NaOH was fraught by flooding and other issues due to blocking of the tubes of our electrolyzer by salt from the electrolyte, leading to this sample being unusable for analysis.

tested in CsOH, indicating that perhaps the morphology of the surface $KHCO_3$ deposits leads to a greater frequency of flooding events. The presence of these internal deposits indicates degradation via blockage of the pores of the GDE in addition to loss of active area from surface deposits. These internal deposits may hamper the diffusion of CO_2 to the catalyst layer, as well as CO product diffusion away from the catalyst layer when operating the cell at high current densities.

4. CONCLUSIONS

In this work, we investigate the performance of Ag-coated Sigracet 35 BC GDEs in a range of electrolytes, alkaline (0.5−3 M KOH and 1−3 M CsOH) and neutral (2 M K_2CO_3 and 2 M $KHCO_3$). We determine that the loss of CO FE is due to the formation of solid, carbonate/bicarbonate deposits on the catalyst layer surface, as well as the formation of these deposits within the pores of the MPL and CFS. These internal deposits occur due to the loss of hydrophobicity over time resulting in flooding events. We demonstrate via electrochemical testing in combination with pre- and post-testing characterization using SEM, EDX, and XRD that the rate of formation and subsequent deposition of these deposits on the electrode surface increase with bulk OH^- concentration and with local OH^- concentration produced by the CO_2 reduction reaction. Therefore, operating at high current densities and using a higher molarity electrolyte will increase the rate of degradation; the benefits of high-molarity alkaline electrolyte must be balanced with the increased degradation via carbonate deposits on the GDE. Additionally, we show that the rate of carbonate deposition and catalyst layer occlusion can be slowed but not eliminated by switching the electrolyte cation from K^+ to Cs^+, likely due to the higher solubility of $CsHCO_3$ and lesser hydration of the Cs^+ cation leading to smaller and more well-dispersed deposits on the catalyst layer when using CsOH. Future study of electrolyte-dependent deposit nucleation and

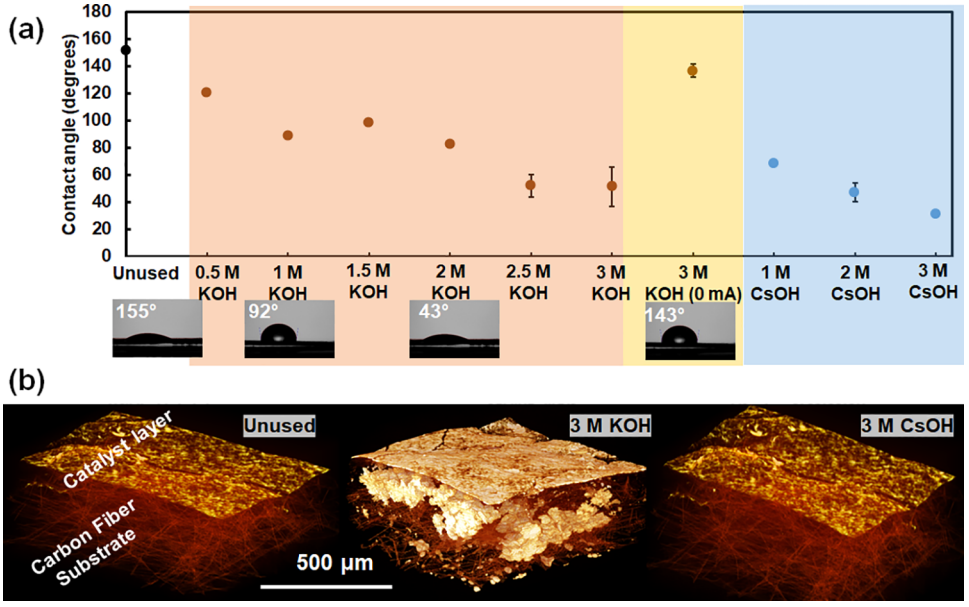

Figure 9. (a) Contact angle data for samples tested in various molarities of KOH and CsOH; the red region highlights samples testing KOH, the yellow region highlights the sample testing in KOH without the application of current, and the blue region highlights the samples tested in CsOH. Increasing molarity (and associated increased carbonate deposits) correlates with a decrease in contact angle. (b) Micro-CT images of unused GDE (left), GDE tested in 3 M KOH for 6 h at −200 mA cm^{-2} (middle), and GDE tested in 3 M CsOH for 6 h at −200 mA cm^{-2} (right). The presence of potassium or cesium on the catalyst layer and within the MPL and CFS of the electrode substrate is visible as bright regions of high density.

https://doi.org/10.1021/acsami.0c21997
ACS Appl. Mater. Interfaces 2021, 13, 15132−15142

growth kinetics can provide more insights into the specific mechanisms controlling morphology and growth rate in each electrolyte.

To study the formation of these deposits more effectively, future work could be done to develop an in situ cell and setup such as those using atomic force microscopy (AFM) by Huang et al. and Shen et al. on solid electrolyte interphases for lithium-ion batteries.[39,40] Recently, a study of Cu-coated GDEs via in situ surface-enhanced Raman spectroscopy was undertaken by our lab and others; this setup could similarly be adapted for future study.[41]

Moving forward, we can see several paths to enhanced durability for alkaline flow systems. First, although preliminary attempts to remove these deposits via rinsing in water and sonication in acetic acid after 6 h of testing were unsuccessful (Figure S10), more frequent and earlier periodic rinsing with water/acidic electrolytes during operation could prevent deposits from growing and remove deposits that are not strongly adhered to the surface. Second, engineering the surface of the catalyst layer via membrane/binder composition or physical nanostructuring could prevent carbonates from the electrolyte from depositing and nucleating larger crystals on the catalyst layer surface; some work on self-cleaning electrodes has already been done by Weng et al. and others.[42] In other works, we have applied a 5 μm overlayer of Sustainion to our Ag-coated GDEs, which inhibited the formation of carbonates in the surface; tailoring binder composition and placement could be key to solving this durability challenge.[43] Third, the electrolyte itself could be engineered to prevent the formation of carbonate compounds.

Elaborating on the third point, as previously mentioned, we have seen in this study that GDEs tested in CsOH exhibit smaller and more evenly dispersed deposits when compared to those tested in KOH. Since KOH is less expensive than CsOH, it would be worthwhile to test if the durability benefits of this CsOH electrolyte are still present or even enhanced when mixed in a variety of concentrations with KOH; we have seen the benefits of this type of electrolyte engineering in previous work.[16,29] Additionally, other instances have been reported, where the addition of an inhibiting agent has prevented the formation of carbonates in the water treatment and oil-refining fields;[44−47] exploring the potential for the use of inhibitor additives in alkaline electrolytes could be a promising avenue of study. Mitigating the carbonate problem will allow us to focus on other degradation issues that may impact GDEs at longer time scales and will ensure that operation in alkaline conditions is viable for long-term CO_2 electrolysis. To implement alkaline flow electrolyzers for ECO_2R on a wider scale, this crucial performance barrier must be overcome.

■ ASSOCIATED CONTENT

Supporting Information

The Supporting Information is available free of charge at https://pubs.acs.org/doi/10.1021/acsami.0c21997.

FE calculation, flow correction factor information, flow cell schematic, CO FE data, image analysis information, KOH cathode potentials, deposit morphology, CsOH cathode potentials, KOH vs CsOH CO FE decline, KOH vs CsOH EDX surface mapping data, SEM of GDEs used with other electrolytes, and SEM of electrode surface post acetic acid treatment (PDF)

■ AUTHOR INFORMATION

Corresponding Author

Paul J. A. Kenis − *Department of Chemical and Biomolecular Engineering, University of Illinois at Urbana-Champaign, Urbana, Illinois 61801, United States;* orcid.org/0000-0001-7348-0381; Email: kenis@illinois.edu

Authors

Emiliana R. Cofell − *Department of Chemical and Biomolecular Engineering and Department of Materials Science and Engineering, University of Illinois at Urbana-Champaign, Urbana, Illinois 61801, United States*

Uzoma O. Nwabara − *Department of Chemical and Biomolecular Engineering, University of Illinois at Urbana-Champaign, Urbana, Illinois 61801, United States*

Saket S. Bhargava − *Department of Chemical and Biomolecular Engineering, University of Illinois at Urbana-Champaign, Urbana, Illinois 61801, United States*

Danielle E. Henckel − *Department of Chemical and Biomolecular Engineering, University of Illinois at Urbana-Champaign, Urbana, Illinois 61801, United States*

Complete contact information is available at: https://pubs.acs.org/10.1021/acsami.0c21997

Notes

The authors declare no competing financial interest.

■ ACKNOWLEDGMENTS

The authors gratefully acknowledge Shell's New Energies Research and Technology (NERT) program for providing funding for this work. The authors would also like to acknowledge the NERT's Dense Energy Carrier (DEC) team for their valuable inputs and discussions during the course of this work. The authors would also like to acknowledge the International Institute of Carbon Neutral Energy Research (WPI-I2CNER) sponsored by the Japanese Ministry for Education, Culture, Sports, Science and Technology and the SURGE Fellowship for the funding of EC. The authors would like to acknowledge Dr. Andrew A. Gewirth and Stephanie Chen, and Zachary Park for their insightful feedback and assistance during this project. Characterization was carried out in the following facilities: Fredrick Seitz Materials Research Laboratory and in the Beckmann Institute for Advanced Science and Technology Imaging Technology Group, University of Illinois at Urbana-Champaign.

■ REFERENCES

(1) Hori, Y. Electrochemical CO_2 Reduction on Metal Electrodes. In *Modern Aspects of Electrochemistry*; Springer: New York, NY, 2008; Vol. *42*, pp 89−189.

(2) Oerlemans, J. Extracting a Climate Signal from 169 Glacier Records. *Science* **2005**, *308*, 675−677.

(3) Hansen, J.; Kharecha, P.; Sato, M.; Masson-Delmotte, V.; Ackerman, F.; Beerling, D.; Hearty, P. J.; Hoegh-Guldberg, O.; Hsu, S.-L.; Parmesan, C.; Rockstrom, J.; Rohling, E. J.; Sachs, J.; Smith, P.; Steffen, K.; Van Susteren, L.; von Schuckmann, K.; Zachos, C. Assessing "dangerous climate change": Required reduction of carbon emissions to protect young people, future generations and nature. *PLoS One* **2013**, *8*, No. e81648.

(4) Zhao, G.; Huang, X.; Wang, X.; Wang, X. Progress in catalyst exploration for heterogeneous CO_2 reduction and utilization: a critical review. *J. Mater. Chem. A* **2017**, *5*, 21625−21649.

(5) Verma, S.; Hamasaki, Y.; Kim, C.; Huang, W.; Lu, S.; Jhong, H.-R. M.; Gewirth, A. A.; Fujigaya, T.; Nakashima, N.; Kenis, P. J. A.

Insights into the Low Overpotential Electroreduction of CO_2 to CO on a Supported Gold Catalyst in an Alkaline Flow Electrolyzer. *ACS Energy Lett.* **2018**, *3*, 193−198.
(6) Zhao, S.; Jin, R.; Jin, R. Opportunities and challenges in CO_2 reduction by gold- and silver-based electrocatalysts: from bulk metals to atomically precise nanoclusters. *ACS Energy Lett.* **2018**, *3*, 452−462.
(7) Hoang, T. T. H.; Verma, S.; Ma, S.; Fister, T. T.; Timoshenko, J.; Frenkel, A. I.; Kenis, P. J. A.; Gewirth, A. A. Nanoporous copper-silver alloys by additive-controlled electrodeposition for the selective electroreduction of CO_2 to CO. *J. Am. Chem. Soc.* **2018**, *140*, 5791−5797.
(8) Kutz, R. B.; Chen, Q.; Yang, H.; Sajjad, S. D.; Liu, Z.; Masel, I. R. Sustainion Imidazolium-Functionalized Polymers for Carbon Dioxide Electrolysis. *Energy Technol.* **2017**, *5*, 929−936.
(9) Dinh, C.-T.; Burdyny, T.; Kibria, M. G.; Seifitokaldani, A.; Gabardo, C. M.; Garcia de Arquer, F. P.; Kiani, A.; Edwards, J. P.; De Luna, P.; Bushuyev, O. S. B.; Zou, C.; Quintero-Bermudez, R.; Pang, Y.; Sinton, D.; Sargent, E. H. CO_2 electroreduction to ethylene via hydroxide-mediated copper catalysis at an interface. *Science* **2018**, *360*, 783−787.
(10) Kim, B.; Hillman, F.; Ariyoshi, M.; Fujikawa, S.; Kenis, P. J. A. Effects of composition of the micro porous layer and the substrate on performance in the electrochcemical reduction of CO_2 to CO. *J. Power Sources* **2016**, *312*, 192−198.
(11) Weng, L.-C.; Bell, A. T.; Weber, A. Z. Modeling Gas Diffusion Electrodes for CO_2 Reduction. *Phys. Chem. Chem. Phys.* **2018**, *20*, 16973−16984.
(12) Verma, S.; Kim, B.; Jhong, H.-R. M.; Ma, S.; Kenis, P. J. A. A Gross-Margin Model for Defining Technoeconomic Benchmarks in the Electroreduction of CO_2. *ChemSusChem* **2016**, *9*, 1972−1979.
(13) Spurgeon, J.; Kumar, B. A comparative technoeconomic analysis of pathways for commercial electrochemical reduction of CO_2 to liquid products. *Energy Environ. Sci.* **2018**, *11*, 1536−1551.
(14) Jouny, M.; Luc, W.; Jiao, F. General Technoeconomic Analysis of CO_2 Electrolysis Systems. *Ind. Eng. Chem. Res.* **2018**, *57*, 2165−2177.
(15) Nwabara, U. O.; Cofell, E.; Verma, S.; Negro, E.; Kenis, P. J. A. Durable Cathodes and Electrolyzers for the Efficient Aqueous Electrochemical Reduction of CO_2. *ChemSusChem* **2020**, *13*, 855−875.
(16) Bhargava, S. S.; Proietto, F.; Azmoodeh, D.; Cofell, E. R.; Henckel, D. A.; Verma, S.; Brooks, C. J.; Gewirth, A. A.; Kenis, P. J. A. System Design Rules for Intensifying the Electrochemical Reduction of CO_2 to CO on Ag Nanoparticles. *ChemElectroChem* **2020**, *7*, 2001−2011.
(17) Gabardo, C. M.; Seifitokaldani, A.; Edwards, J. P.; Dinh, C.-T.; Burdyny, T.; Kibria, M. G.; O'Brien, C. P.; Sargent, E. H.; Sinton, D. Combined high alkalinity and pressurization enable efficient CO_2 electroreduction to CO. *Energy Environ. Sci.* **2018**, *11*, 2531−2539.
(18) Bang, J.-H.; Jang, Y. N.; Kim, W.; Song, K. S.; Jeon, C. W.; Chae, S. C.; Lee, S.-W.; Park, S.-J.; Lee, M. G. Precipitation of calcium carbonate by carbon dioxide microbubbles. *Chem. Eng. J.* **2011**, *174*, 413−420.
(19) Schulz, K. G.; Riebesell, U.; Rost, B.; Thoms, S.; Zeebe, R. E. Determination of the rate constants for the carbon dioxide to bicarbonate inter-conversion in pH-buffered seawater systems. *Mar. Chem.* **2006**, *100*, 53−65.
(20) Gülzow, E. Alkaline fuel cells: a critical view. *J. Power Sources 61* 99 104. DOI: 10.1016/S0378-7753(96)02344-0.
(21) Lafforgue, C.; Zadick, A.; Dubau, L.; Maillard, F.; Chatenet, M. Selected review of the degradation of Pt and Pd-based carbon-supported electrocatalysts for alkaline fuel cells: towards mechanisms of degradation. *Fuel Cells* **2018**, *18*, 229−238.
(22) Wu, J.; Yuan, X. Z.; Martin, J.; Wang, H.; Zhang, J.; Shen, J.; Wu, S.; Merida, W. A review of PEM fuel cell durability: Degradation mechanisms and mitigation strategies. *J. Power Sources* **2008**, *184*, 104−119.
(23) Naughton, M. S.; Brushett, F. R.; Kenis, P. J. A. Carbonate resilience of flowing electrolyte-based alkaline fuel cells. *J. Power Sources* **2011**, *196*, 1762−1768.
(24) Jovanovic, S.; Krause, R.; Luken, A.; Ackermann, J.; Merz, S.; Jakes, P.; Eichen, R.-A.; Granwehr, J. Post-test Raman investigation of silver based gas diffusion electrodes. *J. Electrochem. Soc.* **2020**, *167*, No. 086505.
(25) Leonard, M.; Clarke, L. E.; Forner-Cuenca, A.; Brown, S. M.; Brushett, F. Investigating Electrode Flooding in a Flowing Electrolyte, Gas-Fed Carbon Dioxide Electrolyzer. *ChemSusChem* **2020**, *13*, 400−411.
(26) Rabinowitz, J. A.; Kanan, M. W. The future of low-temperature carbon dioxide electrolysis depends on solving one basic problem. *Nat. Commun.* **2020**, *11*, No. 5231.
(27) Jhong, H.-R. M.; Brushett, F. R.; Kenis, P. J. A. The Effects of Catalyst Layer Deposition Methodology on Electrode Performance. *Adv. Energy Mater.* **2013**, *3*, 589−599.
(28) Resh, H. M. *Hydroponic Food Production.*; CRC Press: Boca Raton, FL, 2013.
(29) Verma, S.; Lu, X.; Ma, S.; et al. The effect of electrolyte composition on the electroreduction of CO_2 to CO on Ag-based gas diffusion electrodes. *Phys. Chem. Chem. Phys.* **2016**, *18*, 7075−7084.
(30) Thorson, M.; Siil, K. I.; Kenis, P. J. A. Effect of Cations on the Electrochemical Conversion of CO_2 to CO. *J. Electrochem. Soc.* **2013**, *160*, F69.
(31) Cesium Bicarbonate. https://pubchem.ncbi.nlm.nih.gov/compound/Cesium-bicarbonate (accessed 2020-11-18).
(32) Schultz, H.; Bauer, G.; Schachl, E.; Hagedorn, F.; Schmittinger, P. Potassium Compounds. In *Ullmann's Encyclopedia of Industrial Chemistry*; Wiley: New York, NY, 2000.
(33) Gilliam, R. J.; Graydon, J. W.; Kirk, D. W.; Thorpe, S. J. A review of specific conductivities of potassium hydroxide solutions for various concentrations and temperatures. *Int. J. Hydrogen Energy* **2007**, *32*, 359−364.
(34) Potassium Bicarbonate. https://pubchem.ncbi.nlm.nih.gov/compound/Potassium-bicarbonate (accessed 2020-11-18).
(35) Potassium Carbonate. https://pubchem.ncbi.nlm.nih.gov/compound/Potassium-carbonate (accessed 2020-11-18).
(36) Liu, J.; Talarposhti, M. R.; Asset, T.; Sabarairajan, D. C.; Y, P. D.; Atanassov, P.; Zenyuk, I. V. Understanding the role of interfaces for water management in platinum-group metal free electrodes in polymer electrolyte fuel cells. *ACS Appl. Energy Mater.* **2019**, *2*, 3542−3553.
(37) Nishida, K.; Murakami, T.; Tsushima, S.; Hirai, S. Measurement of liquid water content in cathode gas diffusion electrode of polymer electrolyte fuel cell. *J. Power Sources* **2010**, *195*, 3365−3373.
(38) Schröder, D.; Laue, V.; Krewer, U. Numerical simulation of gas-diffusion electrodes with moving gas-liquid interface: A study on pulse-current operation and electrode flooding. *Comput. Chem. Eng.* **2016**, *84*, 217−225.
(39) Huang, S.; Cheong, L.-Z.; Wang, S.; Wang, D.; Shen, C. In-situ Study of Surface Structure Evolution of Silicon Anodes by Electrochemical Atomic Force Microscopy. *Appl. Surf. Sci.* **2018**, *452*, 67−74.
(40) Shen, C.; Wang, S.; Jin, Y.; Han, W.-Q. In Situ AFM Imaging of Solid Electrolyte Interfaces on HOPG with Ethylene Carbonate and Fluoroethylene Carbon-Based Electrolytes. *ACS Appl. Mater. Interfaces* **2015**, *7*, 25441−25447.
(41) Henckel, D. A.; Counihan, M. J.; Holmes, H. E.; Chen, X.; Nwabara, U. O.; Verma, S.; Rodriguez-Lopez, J.; Kenis, P. J. A.; Gewirth, A. A. Potential Dependence of the Local pH in a CO_2 Reduction Electrolyzer. *ACS Catal.* **2021**, *11*, 255−263.
(42) Weng, Z.; Zhang, X.; Wu, Y.; Huo, S.; Jiang, J.; Liu, W.; He, G.; Liang, Y.; Wang, H. Self-cleaning catalyst electrodes for stabilized CO_2 reduction to hydrocarbons. *Angew. Chem., Int. Ed.* **2017**, *56*, 13135−13139.
(43) Nwabara, U. O.; Hernandez, A. D.; Henckel, D. H.; Chen, X.; Cofell, E. R.; deHeer, M. P.; Verma, S.; Gewirth, A. A.; Kenis, P. J. A.

Binder-focused approaches to improve stability of cathodes for CO_2 electroreduction. Submitted (under review), 2021.
(44) Gal, J.-Y.; Bollinger, J.-C.; Tolosa, H.; Gache, N. Calcium carbonate solubility: a reappraisal of scale formation and inhibition. *Talanta* **1996**, *43*, 1497−1509.
(45) Bischoff, J. L.; Fyfe, W. S. Catalysis, inhibition, and the calcite-aragonite problem; [Part] 1, The calcite-aragonite transformation. *Am. J. Sci.* **1968**, *266*, 65−79.
(46) Lin, Y.-P.; Singer, P. C. Inhibition of calcite crystal growth by polyphosphates. *Water Res.* **2005**, *39*, 4835−4843.
(47) Burton, E. A.; Walter, L. M. The role of pH in phosphate inhibition of calcite and aragonite precipitation rates in seawater. *Geochim. Cosmochim. Acta* **1990**, *54*, 797−808.

https://doi.org/10.1021/acsami.0c21997
ACS Appl. Mater. Interfaces 2021, 13, 15132−15142